



Bone morphogenetic protein 4 thermosensitive hydrogel inhibits corneal neovascularization by repairing corneal epithelial apical junctional complexes

Weijin Nan^{a,c,1}, Sitong Shen^{c,1}, Yongyan Yang^{b,1}, Meiliang Wu^c, Yuxi He^c, Ruiting Zhang^b, Xuejun Cui^{b,d,*}, Yan Zhang^{a,c,**}

^a Department of Ophthalmology, Shanghai General Hospital, Shanghai Jiao Tong University School of Medicine, National Clinical Research Center for Eye Diseases, Shanghai, 200080, PR China

^b College of Chemistry, Jilin University, Changchun, 130012, PR China

^c Department of Ophthalmology, The Second Hospital of Jilin University, 218 Ziqiang Street, Nangan District, Changchun, Jilin Province, 130041, PR China

^d Weihai Institute for Bionics-Jilin University, Weihai, 264400, PR China

ARTICLE INFO

Keywords:

Bone morphogenetic protein 4
Corneal neovascularization
Poloxamer
Oxidized sodium alginate
Thermosensitive gel
Apical junctional complexes

ABSTRACT

Corneal neovascularization (CNV) is a heavy attribute of blinding disease changes. Existing medications need numerous infusions and have a limited absorption. Investigating novel drugs with safety, efficacy, and convenience is crucial. In this study, we developed a bone morphogenetic protein 4 (BMP4)-loaded poloxamer-oxidized sodium alginate (F127-OSA) thermosensitive hydrogel. The 14 % F127-OSA hydrogel transformed from sol to gel at 31–32 °C, which might extend the application period on the ocular surface. The hydrogel's porous structure and uniform dispersion made it possible for drugs to release gradually. We used a suture-induced rat CNV model to investigate the mechanism of CNV inhibition by hydrogel. We discovered that F127-OSA hydrogel loaded with BMP4 could significantly reduce the length and area of CNV, relieve corneal edema, and stop aberrant epithelial cell proliferation. The hydrogel's efficacy was superior to that of the common solvent group. Additionally, BMP4 thermosensitive hydrogel repaired ultrastructure, including microvilli, intercellular junctions, and damaged apical junctional complexes (AJs), suggesting a potential mechanism by which the hydrogel prevented CNV formation. In conclusion, our investigation demonstrates that F127-OSA thermosensitive hydrogel loaded with BMP4 can repair corneal epithelial AJs and is a promising novel medication for the treatment of CNV.

1. Introduction

The cornea is normally a transparent, avascular tissue that is the first barrier to the surface of the eye [1]. A variety eye conditions, such as trauma, corneal infection, and chemical burn, can cause the capillaries and venules in the cornea's peripheral vascular network to branch out and invade the avascular cornea [2,3]. Contact lenses use also raises the incidence of CNV [4]. CNV is the fourth most common cause of vision impairment globally and is a significant pathogenic change that can cause blindness [5]. However, the current treatment of CNV has some limitations. For instance, corneal transplantation may cause rejection.

Drug therapy is a widely used and simple approach, but it comes with a number of drawbacks. Medication residence time on the ocular surface is insufficient, bioavailability is limited [6], and frequent drug delivery is required due to factors such as tears, blinking, and corneal anatomy [7]. In addition, glaucoma and cataract are easily brought on by long-term hormone usage. Although bevacizumab can cure CNV, subconjunctival injection of the drug slows the recovery of corneal sensitivity in experimental models of alkali burn and impairs corneal epithelial wound repair and nerve regeneration [8]. Therefore, it is critical to investigate novel medications with safety, effectiveness, convenience and efficiency for the treatment of CNV.

* Corresponding author. . College of Chemistry, Jilin University, Changchun, 130012, PR China.

** Corresponding author. Department of Ophthalmology, Shanghai General Hospital, Shanghai Jiao Tong University School of Medicine, National Clinical Research Center for Eye Diseases, Shanghai, 200080, PR China.

E-mail addresses: cui_xj@jlu.edu.cn (X. Cui), ahzhangyolanda@163.com (Y. Zhang).

¹ Weijin Nan, Sitong Shen and Yongyan Yang contributed equally to this work.

<https://doi.org/10.1016/j.mtbio.2024.100944>

Received 20 September 2023; Received in revised form 16 December 2023; Accepted 2 January 2024

Available online 4 January 2024

2590-0064/© 2024 Published by Elsevier Ltd. This is an open access article under the CC BY-NC-ND license (<http://creativecommons.org/licenses/by-nc-nd/4.0/>).

Corneal epithelium AJCs is a key structure to maintain corneal barrier function. It is made up of adherens junctions underneath the corneal epithelial cells and tight junctions at the top. AJCs can control cellular polarity, paracellular ion and macromolecule transport, and intercellular interaction [9]. The various etiologic factors that lead to CNV also produce varying degrees of damage to corneal epithelial AJCs. Inflammatory cell infiltration and CNV formation were seen in corneal epithelial injury caused by UV [10], alkali burn [11], and EB virus-associated keratitis [12], together with reduced expression of the adherens junction proteins E-cadherin and β -catenin and the tight junction proteins ZO-1 and occludin. Damage to AJCs can further accelerate the development of CNV. When ZO-1 antibody was utilized to interfere with the corneal epithelium's tight junction function, inflammatory cell infiltration and CNV both considerably increased. Vascular endothelium growth factor A (VEGF-A) and angiopoietin have been significantly up-regulated during functional mutations of adherens connexin β -catenin, leading to keratoma and CNV formation [13]. Therefore, preserving the cornea's normal structure and function depends on having intact AJCs, and repairing damaged epithelial AJCs aids in preventing the formation of CNV.

BMP4 acts as a cytokine involved in cell differentiation, proliferation, metastasis and apoptosis, and plays a specific regulatory role in tissue healing and angiogenesis [14–16]. We previously discovered that BMP4 may greatly reduce CNV formation, down-regulate VEGF-A expression, and facilitate corneal epithelial healing [17]. However, the mechanism by which BMP4 plays the role of inhibiting CNV formation is still unclear. Furthermore, due to the limited bioavailability of conventional eye drops, it is unable to fully utilize BMP4 eye drops' biological function.

Hydrogel is a unique three-dimensional structure with a large porosity that can accommodate small molecules and high polymers, etc. By modifying the density and affinity of crosslinking agents, hydrogels can modify their stiffness, viscoelasticity, pore size, and other physical and chemical properties to achieve applications in various fields. Hydrogel's pore structure offers the necessary guarantee for drug loading and release, making it an excellent carrier for drug loading [18, 19]. Therefore, we loaded BMP4 in Poloxamer-407 (pluronic F127) thermosensitive hydrogel, extending the drug's residence duration on the cornea and increasing its usage efficiency. We discovered that compared to BMP4 eye drops alone, BMP4 thermosensitive hydrogel had a stronger inhibitory impact on CNV [20]. In this study, we introduced OSA, which may significantly lower the dosage of F127 and more efficiently save costs. In contrast to F127, F127-OSA has a porous structure that facilitates continuous medication release on the ocular surface. The purpose of this work is to investigate the efficacy of the modified BMP4 thermosensitive hydrogel in preventing CNV development and elucidating its mechanism. Our findings imply that F127-OSA gel loaded with BMP4 can repair corneal epithelial AJCs and is a promising medication for the treatment of CNV.

2. Materials and methods

2.1. Preparation and oxidation degree determination of OSA

The synthesis of OSA is slightly improved on the basis of the original procedure [21]. After thoroughly dissolving 1.0 g of sodium alginate (SA, Tianjin Guangfu Technology Development Co., Ltd., China) in 50 ml of deionized water, acetic acid (Tianjin Tiantai Chemical Co., Ltd., China) was used to raise the pH to 3 and it was heated in a water bath at 40 °C. Afterward, 0.99 g of sodium periodate (NaIO_4 , Shanghai Macklin Biochemical Co., Ltd., China) was added, and the mixture was left without light for 6 h. Then, 1 ml of glycol (Tianjin Tiantai Chemical Co., Ltd., China) was added to stop the reaction once the reaction was finished. The reaction solution was mixed with the ethanol solution to collect the sediment. Finally, pure OSA was obtained by dissolving the collected white precipitate in deionized water, dialysis, and

freeze-drying.

According to the literature, the oxidation degree of OSA was calculated by titration of hydroxylamine hydrochloride (Shanghai Macklin Biochemical Co., Ltd., China) [22]. The 0.05 g sample was dissolved in 15 ml of deionized water, and the pH was adjusted by H_2SO_4 (Sinopharm Chemical Reagent Co., Ltd., China) to 4.5. 0.215 g of hydroxylamine hydrochloride was dissolved in 10 ml of deionized water, with the pH 4.5. Following their total dissolution, the two were mixed and swirled for 24 h. The HCl generated by the reaction with 0.1 M NaOH was then titrated using methyl orange (Sinopharm Chemical Reagent Co., Ltd., China) as an indicator.

$$\text{CHO} (\%) = \frac{(V_2 - V_1) \times c \times M}{m} \times 100\%$$

V_1 and V_2 are the NaOH volumes consumed by blank test (unoxidized alginate) and product (oxidized alginate), respectively. c : NaOH standard solution concentration; M : molar mass of oxidized alginate repeat unit; m : sample quality.

$$\text{CHO} (\%) = \frac{(1.50 - 0.75) \times 0.1 \times 216.1230}{0.05 \times 1000} \times 100\% = 32.42\%$$

2.2. Gel preparation

2.2.1. F127-CDI

12.6 g of pluronic F127 (Lutrol, Basf, Germany) was dissolved in 15 ml of acetonitrile (Sinopharm Chemical Reagent Co., Ltd., China); 1.62 g of N, N'-Carbonyldiimidazole (CDI, Shanghai Macklin Biochemical Co., Ltd., China) was dissolved in 15 ml of acetonitrile and kept from oxidizing by N_2 . After being dissolved, CDI was added to the F127 solution, and the reaction proceeded for 12 h. Following the reaction, the solution was dialyzed for 3 days (MWCO: 3500 D), with deionized water being replaced every 4 h. The freeze-dried white solid F127-CDI was obtained after dialysis was finished.

2.2.2. F127-NH₂

After dissolving 12.6 g of F127-CDI in 15 ml of acetonitrile at room temperature, 10 ml of ethylenediamine (Sinopharm Chemical Reagent Co., Ltd., China) was added. The aforementioned dialysis procedures were repeated and freeze-dried after the response, which lasted overnight.

2.2.3. F127-OSA

After dissolving 10.0 g of F127-NH₂ in 60 ml of deionized water, 0.52 g of OSA was added. The reaction lasted 12 h, and the previous dialysis stages were repeated and freeze-dried.

2.3. Characterization of F127-OSA thermosensitive gel

2.3.1. Fourier transform infrared spectroscopy

By scanning with a Fourier transform infrared spectroscopy (FTIR; IRAffinity-1, Japan) and using the potassium bromide pressing technique, the spectra of 4000–400 cm^{-1} were obtained at room temperature with a resolution of 4 cm^{-1} .

2.3.2. ¹H nuclear magnetic resonance spectroscopy

F127-CDI, F127-NH₂ and F127-OSA were analyzed using Avance NEO 400 NMR spectrometer with D_2O as hydrogenating solvent at 400 MHz.

2.3.3. SEM

Hydrogel morphology was investigated using emission SEM (Hitachi, H-7500, Japan). The dried hydrogel sample was adhered to the double-sided conductive adhesive, plated with platinum for 2 min in an ion sputtering coater, and then analyzed by SEM.

2.4. Rheological property

The rheological characteristics of hydrogels were assessed using a rheometer (MCR 301, Anton Paar, Germany) in order to confirm the mechanical properties of hydrogels. The sample was disc-shaped (25 mm diameter, 0.5 mm height). In short, the energy storage modulus (G') and loss modulus (G'') of the hydrogel were measured under different conditions: 1) the change of G' and G'' at a temperature range of 15–40 °C under 1 % oscillatory strain and a frequency of 1 Hz; 2) at 37 °C, the scanning range is 0.1–100 rad/s for dynamic frequency sweeping and 3) the viscosity of the hydrogel with different shear rates (1–100 s⁻¹) was measured at 37 °C.

2.5. Measurement of gel temperature and gel time

The "vial inversion method" was used to calculate the gel temperature and gel time of the F127-OSA hydrogel at various concentrations. In short, place 1 ml of gel in a 20 ml vial in a water bath at different temperatures and observe its gelling state. The gel temperature and gel time are the conditions under which the sample vial is tilted and the gel ceases to flow. Three parallel measurements were made for each group of samples.

2.6. Optical transmittance measurement

The optical transmittance of F127-OSA thermosensitive gel was tested by an ultraviolet-visible spectrophotometer (TU-1810) in the range of 200–800 nm.

2.7. Drug release in vitro

Artificial tears were used to investigate the in vitro release behavior of albumin from bovine serum (BSA; Sinopharm Chemical Reagent Co., Ltd., China) in F127-OSA hydrogel. In a nutshell, 10 mg of BSA was added to 4 ml of F127-OSA hydrogel solution. Then the mixture solution was placed in a constant temperature water bath at 37 °C, and after the sol-gel conversion, 2 ml of artificial tear (CaCl₂-H₂O 0.06 mg/ml, NaHCO₃ 2.18 mg/ml, NaCl 6.7 mg/ml, pH = 7.4) was gradually added to F127-OSA gel. It was then incubated in a shaker at 37 °C at 100 rpm/min 2 ml of the BSA release matrix was removed periodically and the BSA release concentration in the medium was analyzed by UV-Vis spectrophotometry. To maintain the same volume, fresh artificial tears were added right away. By comparing the cumulative recovery of BSA in the release medium at each time point to the total quantity of BSA in the 4 ml hydrogel, the cumulative release percentage was calculated. The cumulative drug release was calculated using the following equation [23]:

$$\text{Cumulative release (\%)} = \frac{V_s \sum_{i=1}^{n-1} C_i + V_0 C_n}{m_0} \times 100$$

V_s is the sample volume (2 ml), V_0 is the initial volume (4 ml), C_i and C_n are the concentration of the drug at the sampling points i and n (mg/ml), and m_0 is the mass of the drug in the hydrogel (mg).

2.8. In vitro toxicity assay

B16-F10 mouse melanoma hypermetastasis cells (Shanghai Zhong Qiao Xin Zhou Biotechnology Co., Ltd., China) were cultured and treated by CCK-8 (Meilunbio, China) to detect the toxicity of F127-OSA thermosensitive hydrogel in vitro. The modified hydrogel with a mass to volume ratio of 14 % was added to DMEM high-sugar medium (Shanghai Zhong Qiao Xin Zhou Biotechnology Co., Ltd., China) containing 10 % fetal bovine serum and 1 % double antibody at a concentration of 0.1 g/ml for 0.5 h after elimination and incubated for 24 h to obtain the extract. Following this, cells were inoculated into 96-well plates at a

density of 8000/ well and incubated for 24 h. The original cell medium was replaced with 100 μl cell culture medium containing 5 % DMSO, hydrogel extract, and cell culture medium per well, respectively, which referred to the positive group, gel group, and normal group ($n = 5$). After incubation for 24 h, 10 μl CCK-8 enhancement solution was added to each well. After 2 h, absorbance at 450 nm was measured by microplate reader (ThermoFisher Scientific, China) and cell survival rate was calculated.

2.9. Animal model of CNV

Female Wistar rats (7–8 weeks old, 200–220 g) were purchased from Liaoning Changsheng biotechnology Co., Ltd. (Liaoning, China) for experiments. The study was approved by the Ethics Committee of Jilin University. The animal experiment strictly adhered to the National Institutes of Health guide for the care and use of Laboratory animals.

The suture method was used to induce rat CNV. Rats were anesthetized by intraperitoneal injection with pentobarbital (30–50 mg/kg). Under the operating microscope, we positioned the cornea with a 4 mm corneal trephine, then we used nylon 10-0 shovel needle to insert the needle from the limbus of cornea about 1.5 mm away, sutured at 4, 8 and 12 o'clock directions of the cornea. The nylon 10-0 shovel needle was used to penetrate the deep corneal stroma without penetrating the endothelium as a stimulus to induce CNV. The rats were then randomly divided into six groups. In the first two groups, we dropped 20 μg/ml BMP4 (R&D Systems, USA) to left eyes as BMP4 group, one drop 5 μl, and reconstitution buffer 4 (0.1 % Bovine Serum Albumin in 4 mM HCl, R&D) to right eyes as solvent control group, one drop 5 μl. In BMP4 thermosensitive hydrogel group, 20 μg/ml of BMP4 was dissolved in F127-OSA hydrogel as solvent, which was administered to the left eyes, one drop 5 μl, and F127-OSA hydrogel was applied to the right eyes as gel control group, one drop 5 μl. Drugs were used three times a day, 5 μl per time for 3, 5 or 7 days. In addition, there was a suture group (no drugs after modeling) for 3, 5 or 7 days, and an untreated group (no suture and no drugs). For the rat models, all of our procedures followed the Association for Research in Vision and Ophthalmology (ARVO) Statement for the Use of Animals in Ophthalmic and Vision Research.

2.10. Biomicroscope examination

The induction of CNV was evaluated by biomicroscope examination at 3, 5, 7 days after the surgical intervention. Slit lamp was used to take clinical photographs at 4 o'clock, 8 o'clock and 12 o'clock directions of the cornea. The length and area of CNV were analyzed using Image J (National Institutes of Health, USA).

2.11. HE staining

Rats were sacrificed following 3, 5 or 7 days of observations. The eyes were removed and set in 4 % paraformaldehyde (Biosharp, China) for 12 h. Corneas were dissected from the ocular bulb, then full corneal cross-sections were obtained and embedded in paraffin. Paraffin sections were stained using hematoxylin and eosin (Department of nephrology, the Second Hospital of Jilin University) and images were collected under microscope.

2.12. TEM

Dissected corneas were fixed in 2.5 % glutaraldehyde (Biosharp, China) at 4 °C for 4 h, post-fixed with 1 % osmium tetroxide. Each sample was subsequently dehydrated at room temperature by adding to solutions of 30 % and then 50 % ethanol, followed by staining with 70 % uranyl acetate at 4 °C for 4 h. The samples were then dehydrated at room temperature with a concentration gradient of 70 %, 90 %, 100 % ethanol for 15 min each immersion and embedded in Spurr resin. Ultrathin sections were made with an ultramicrotome and then stained with lead

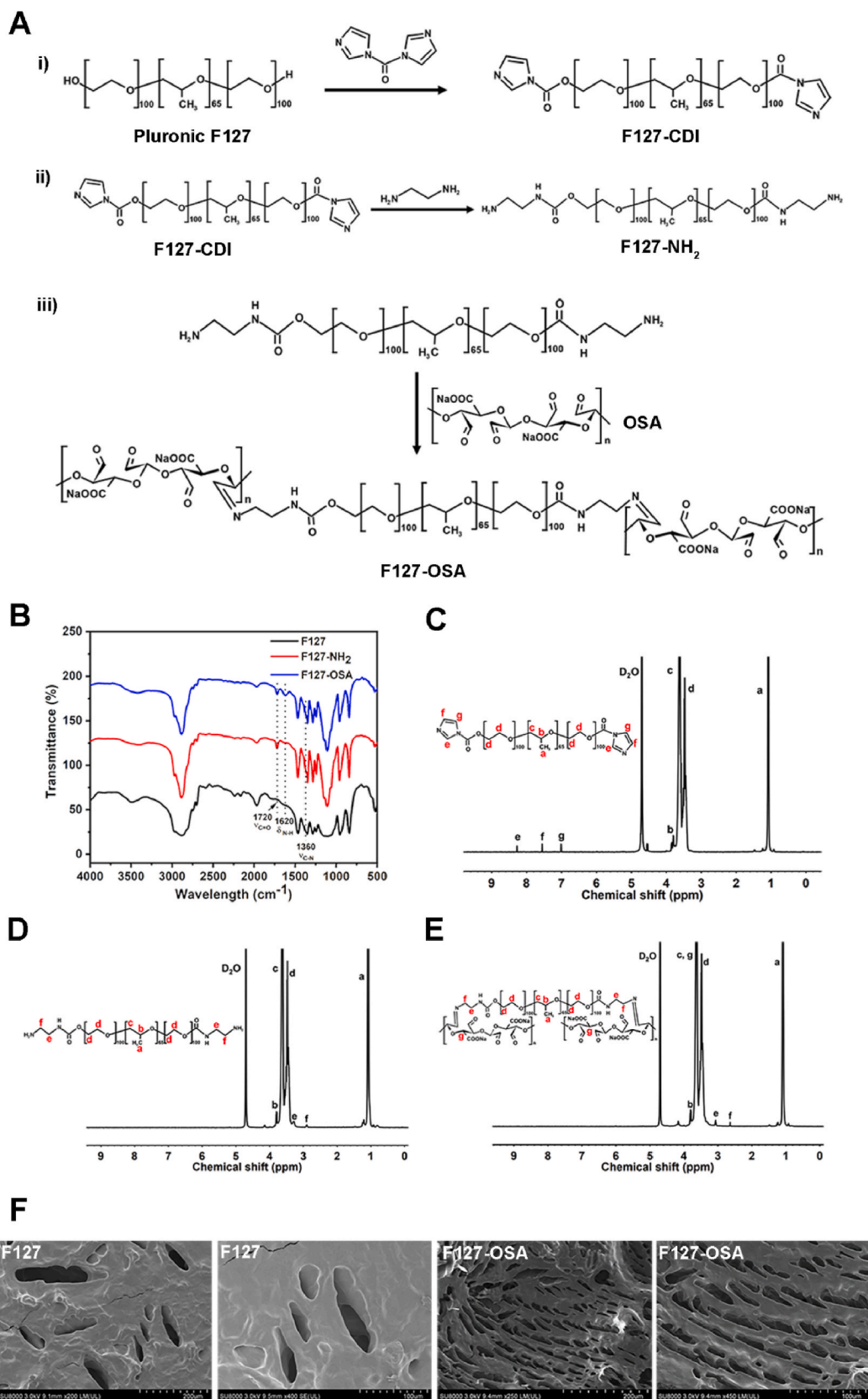


Fig. 1. Synthesis and characterization of F127-OSA thermosensitive hydrogel. (A) Schematic diagram of hydrogel synthesis; (B) FTIR was used to determine the chemical structure of F127, F127-NH₂ and F127-OSA. (C) ¹H NMR spectroscopy of F127-CDI; (D) ¹H NMR spectroscopy of F127-NH₂; (E) ¹H NMR spectroscopy of F127-OSA; (F) Microscopic morphology of F127 and F127-OSA under SEM.

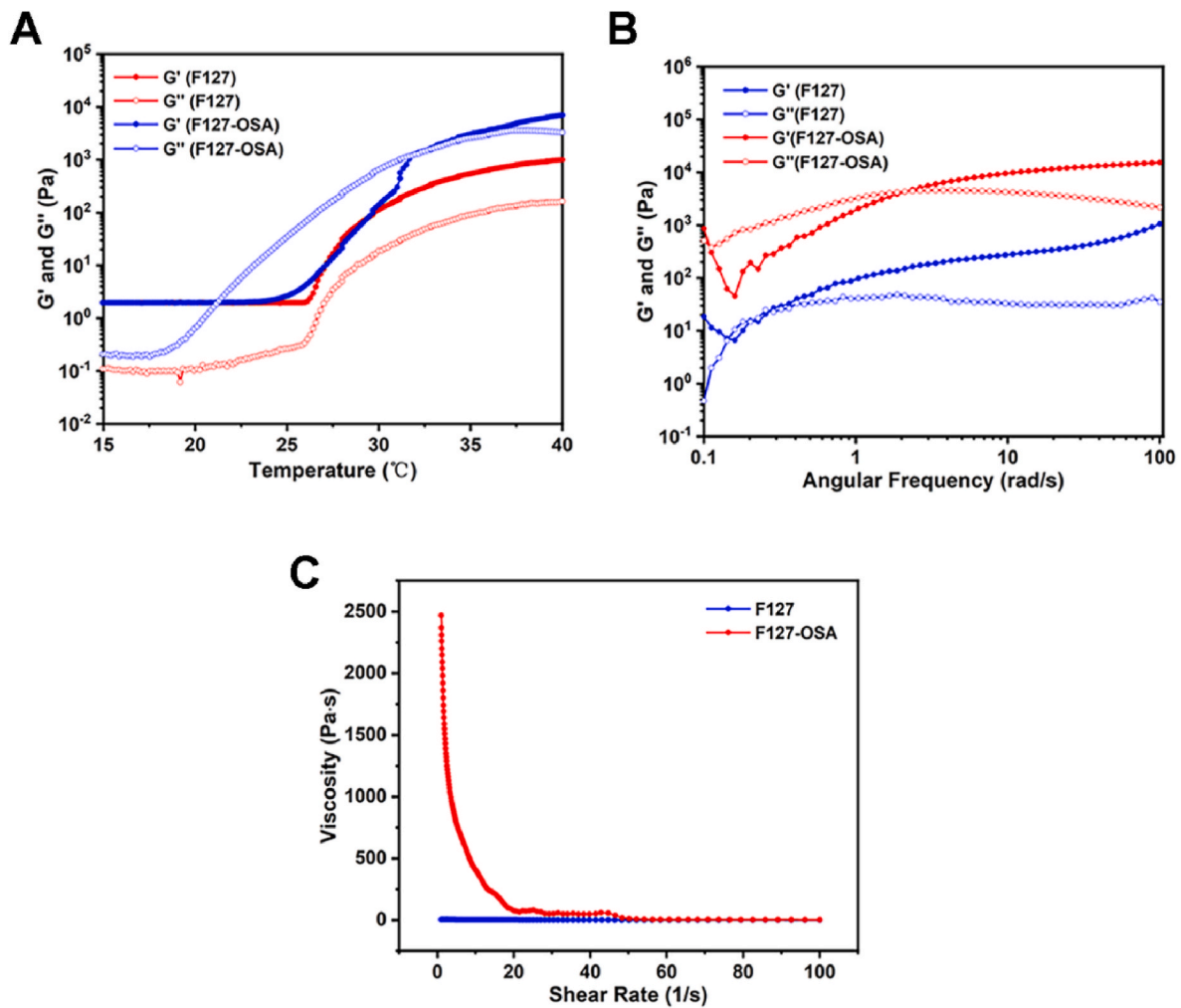


Fig. 2. Rheological properties of F127-OSA thermosensitive hydrogel. (A) the relationship between F127 and F127-OSA hydrogel's modulus and temperature; (B) G' and G'' of F127 and F127-OSA hydrogels in the oscillating frequency range of 0.1–100 rad/s; (C) viscosity change of F127 and F127-OSA hydrogels with shear rate.

citrate to observe the microstructure changes in cornea (Department of nephrology, the Second Hospital of Jilin University).

2.13. Western blot

Rats were sacrificed 3 or 7 days after suturing. The corneas were ground to powder with liquid nitrogen. Total protein was lysed by ultrasonication (Scientz, China) after extracting by RIPA buffer (Beyotime, China) and then centrifuged for protein extraction. After agarose gel electrophoresis, the polyvinylidene fluoride membrane (Merck, Ireland) was blocked with 5 % non-fat milk for 1 h and incubated with primary antibodies against ZO-1 (1:1000, 21773-1-AP, Proteintech, China), E-cadherin (1:1000, 20874-1-AP, Proteintech, China), β -catenin (1:1000, 51067-2-AP, Proteintech, China) and β -actin (1:3000, AC038, ABclonal, China) at 4 $^{\circ}\text{C}$ overnight. The polyvinylidene fluoride membrane was then incubated with the Goat anti-rabbit IgG secondary antibody HRP conjugated (1:10000, #L3012, SAB, USA) for 1 h at room temperature. Protein bands were detected using enhanced chemiluminescence substrate after the membrane was washed. The greyscale value for each protein was normalized to that of β -actin and averaged by Image J software. Each experiment was repeated three times independently.

2.14. Immunofluorescence staining

Rats were sacrificed 3 or 7 days after suturing. The eyes were

removed, and corneas were dissected from the ocular bulb. Corneas were embedded in SAKURA Tissue-Tek[®] O.C.T. compound and sliced at a thickness of 3 μm using a cryostat (Leica CM1950, China). After rewarming the frozen cross sections at room temperature, the sections were fixed in 4 % paraformaldehyde for 20 min, followed by a blocking and permeabilization step for 1 h in PBS with 1 % BSA and 0.5 % Triton-X. Then the sections were incubated with primary antibodies against ZO-1 (1:1000, 21773-1-AP, Proteintech, China), E-cadherin (1:100, 20874-1-AP, Proteintech, China) and β -catenin (1:200, 51067-2-AP, Proteintech, China) at 4 $^{\circ}\text{C}$ overnight. The sections were then incubated with Dylight 488 goat anti-rabbit-IgG (1:500, Abbkine, China) for 1 h at room temperature. DAPI was used as a nuclear counterstain. The sections were photographed under a fluorescence microscope (Olympus, Japan).

2.15. Statistical analysis

The SPSS 23.0 software (IBM SPSS, Inc., United States) was used for statistical analysis. All the data were represented as means \pm standard error of mean (SEM). A P value under 0.05 was considered to be statistically significant.

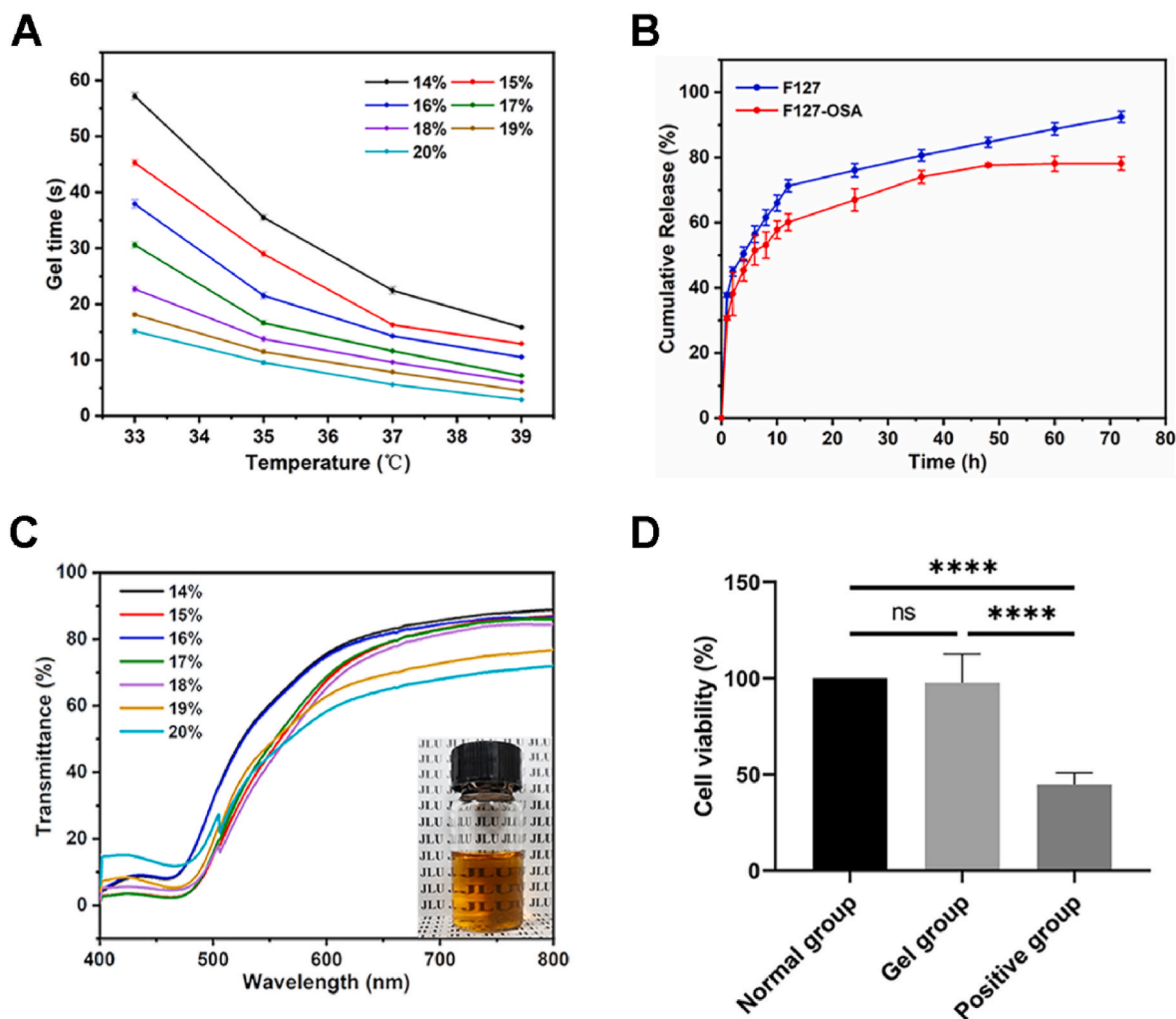


Fig. 3. (A) Gel time and gel temperature of F127-OSA thermosensitive hydrogel with different concentrations. Temperature range:33°C–39 °C. Error bars indicate \pm SEM (n = 3); (B) BSA release spectra of F127 and F127-OSA thermosensitive hydrogels in vitro. Error bars indicate \pm SEM (n = 3); (C) transmittance of F127-OSA at different concentrations; (D) viability of B16–F10 mouse melanoma hypermetastasis cells in normal group, gel group and positive group. ****p < 0.0001 (n = 5).

3. Results and discussion

3.1. Synthesis and characterization of F127-OSA thermosensitive gel

Fig. 1A showed the synthesis scheme of F127-OSA. First, the end group of F127 was activated by CDI, then ethylenediamine was introduced to the F127 molecular chain. Finally, OSA was grafted onto F127–NH₂ chain by Schiff base reaction to obtain F127-OSA polymer. The chemical structure of F127, F127–NH₂, and F127-OSA was ascertained using FTIR. As shown in Fig. 1B, the stretching vibration of C=O had a very broad absorption peak near 1720 cm⁻¹. The absorption peak at 1620 cm⁻¹ could be attributed to the deformation vibration of –NH₂ and overlapped with the asymmetric stretching vibration of the –COO⁻ group. The absorption peak at 1360 cm⁻¹ was caused by the stretching vibration of C–N. NMR analysis showed that protons "e", "f" and "g" of F127-CDI (400 MHz, D₂O, ppm) at δ = 1.09 (d, 3H, –CH₃), 3.30–3.55 (–OCH₂CHO– of propylene oxide and –CH₂CH₂O– of polyethylene oxide), 8.27 (s, 1H), 7.56 (s, 1H) and 7.01 (s, 1H) ppm were imidazole group [24]. A new peak appeared in the NMR hydrogen spectrum of F127–NH₂ (400 MHz, D₂O, ppm), namely 2.90 ppm (t, 2H, –CH₂N–), 3.28 ppm (q, 2H, –CNCH₂–). As a result of the impact of imine bonds, the peaks of –CH₂N– and –CNCH₂– in the ¹H NMR of F127-OSA changed from 2.90 to 3.28 ppm to 2.64 and 3.06 ppm, respectively (Fig. 1C–E). These findings demonstrated that the effective synthesis of F127-OSA.

In order to understand the surface morphology of F127 and F127-osa hydrogels, their micromorphology was investigated using scanning electron microscopy. As shown in Fig. 1F, there was no regular microporous structure on the surface of F127, but F127-OSA fibers were evenly dispersed and joined into a strong network structure, demonstrating a porous structure. This finding supported the hypothesis that OSA grafting affected the morphology of hydrogels. Hydrogels were further proven to be effective medication delivery and storage carriers due to their porous structure.

3.2. Rheological properties

The rheological test results of hydrogels reflect the mechanical properties of hydrogels, which is an important factor affecting their biological applications. Rheological properties include energy storage modulus (G') and loss modulus (G'') [25]. G' and G'' of hydrogel were investigated using small deformation oscillation method. The relationship between the hydrogel's modulus and temperature was depicted in Fig. 2A. In the range of 15–40 °C, when the temperature increased to 31.8 °C, $G' = G''$, the hydrogel transformed from a solution to a gel state, demonstrating the thermal responsiveness of the F127-OSA hydrogel. The G' of the F127-OSA hydrogel grew substantially with frequency at 37 °C in the range of 0.1–100 rad/s. F127-OSA hydrogel had fluidity at low frequency and it was solid at high frequency, with $G' > G''$,

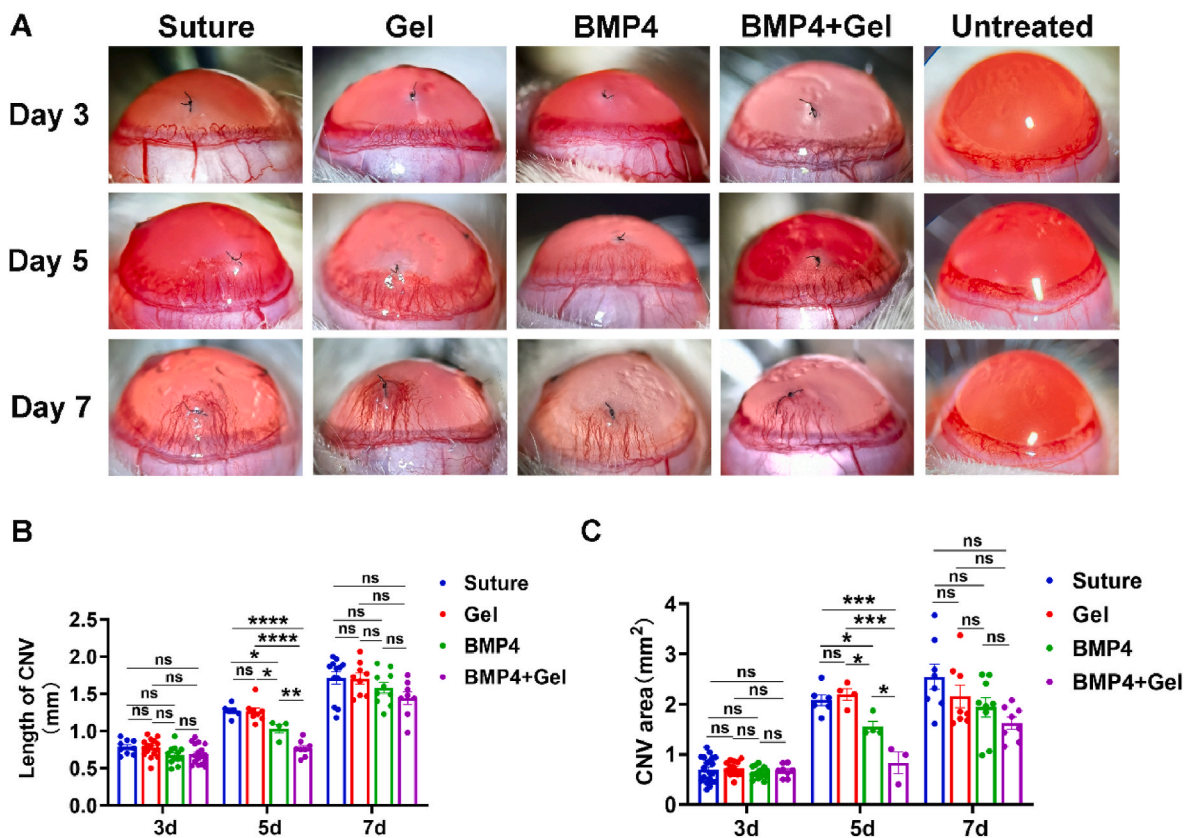


Fig. 4. Inhibition of suture induced CNV by BMP4 and BMP4 thermosensitive gel. (A) Representative slit-lamp images of CNV in suture group, gel group, BMP4 group, BMP4+gel group and untreated group at different times after suturing (magnification: $\times 16$); (B) CNV length between groups at a specific time after modeling; (C) CNV area between groups at a specific time after modeling. The length and area of CNV was quantified and normalized ($n = 6$). Results were presented as means \pm SEM. * $P < 0.05$, ** $P < 0.01$, *** $P < 0.001$, and **** $P < 0.0001$.

exhibiting the properties of reversible gel (Fig. 2B). Previous research has demonstrated that vitreous substitutes with G' greater than 100 Pa could withstand high reversible deformation resistance when subjected to traumatic stress [26]. Additionally, the hydrogel's viscosity was examined. As can be seen from Fig. 2C, the viscosity of F127-OSA hydrogel was significantly higher than that of F127 at 37 °C. The hydrogel's viscosity dropped dramatically with an increase in shear rate, going from 2470 Pa s to 2.50 Pa s, while the shear rate changed from 1 to 100 s^{-1} , proving that it was both shear thinnable and injectable.

3.3. Gel temperature and gel time analysis

The optimal eye hydrogel should be able to flow easily at low temperatures, solidify when it comes in touch with the eye's surface, and continue to be gel even after the maximum dilution of tears. Poloxamer is a substance that is frequently used for in situ gel production. It is a copolymer composed of polyethylene oxide (PEO) and propylene oxide (PPO) units. When the temperature rises, the Poloxamer PPO unit dehydrates to create micellar nuclei, and the PEO unit is hydrated, the micellar nuclei expand to form the outer structures [27]. F127-OSA micelles will arrange to form hydrogels as the temperature rises.

The "vial inversion method" was used to determine the gel formation time and gel formation temperature of F127-OSA hydrogel at different concentrations. F127-OSA hydrogels with different mass fractions were dissolved in deionized water at low temperature before being incubated in a constant temperature bath. The experimental results showed that gel could not be formed when the gel concentration was less than 14 %. As shown in Fig. 3A, the gel time of all hydrogel groups decreased with increasing concentration. The rapid formation of hydrogel could effectively avoid protein drug loss, extend the duration of drug activity on the

ocular surface, and improve the therapeutic effect. It was discovered that 14 % of the F127-OSA hydrogel started to transition from the sol to gel state at 31 °C. The hydrogel went back to its sol state when the room temperature fell below the gel temperature. OSA enhanced PEO's hydration and had good hydrophilicity. The intermolecular distance decreased as temperature rose, which facilitated the creation of hydrogen bonds and accelerated the production of hydrogels. It is helpful to prolong the duration of the drug on the ocular surface, reduce the drug loss and improve the therapeutic effect.

3.4. Drug release in vitro

One of the primary methods for evaluating a medication's behavior in vivo is by measuring the in vitro release rate of the drug inside a formulation [28]. The cumulative release and release behavior of the drug from F127-OSA hydrogel in artificial tears were studied using BSA as a drug model. Fig. 3B displayed the F127 and F127-OSA hydrogel release curves. Because F127 was in a semi-fluid condition at a concentration of 14 % and was unable to adequately encapsulate the medication in its porous structure, the release quantity of F127 reached 92 % in the 48 h when compared to the release curves of F127-OSA. The drug release of F127-OSA reached 78 % at 72 h under the same circumstances, and the cumulative release was at its lowest within that time. This helped to achieve continuous medication release on the surface of the cornea without causing discomfort to the patient owing to the drug's abrupt release. The results were consistent with the porous structure of F127-OSA hydrogel under SEM. In subsequent experiments, after BMP4 was loaded on F127-osa, the residual aldehyde group of OSA may react with the amino group on BMP4, but the amount of residual aldehyde group of OSA should be very small, because the degree of

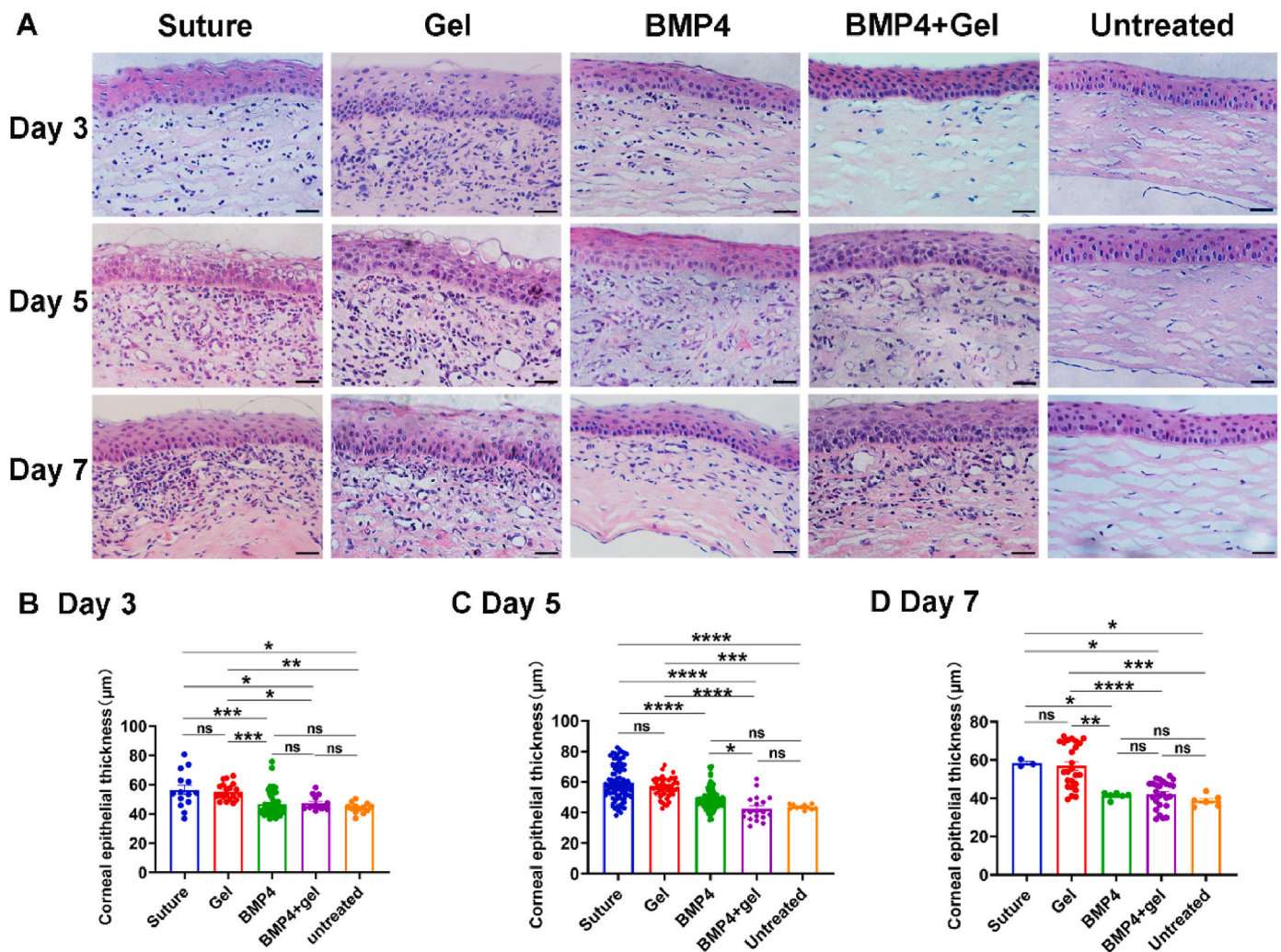


Fig. 5. Effects of BMP4 and BMP4 thermosensitive hydrogel on corneal epithelial thickness and epithelial cell arrangement. (A) HE slices from suture group, gel group, BMP4 group, BMP4+gel group and untreated group at different times after modeling; (B) corneal epithelial thickness of each group at Day 3; (C) corneal epithelial thickness of each group at Day 5; (D) corneal epithelial thickness of each group at Day 7. Scale bars = 20 µm (× 400). n = 6, results were presented as means ± SEM. *P < 0.05, **P < 0.01, ***P < 0.001, and ****P < 0.0001.

oxidation measured when doing oxidation at that time was not very high. And in the later reaction process the reactants are added by molar ratio, generally there will not be too much residue, which has little effect on the release of BMP4. The porous structure of F127-OSA hydrogel can make BMP4 release gradually.

3.5. Light transmittance and in vitro toxicity

Transparency is essential for a good visual outcome since the cornea is a transparent, avascular tissue [29]. By using a UV-Vis spectrophotometer, the optical transmittance of F127-OSA hydrogel in the 200–800 nm region was investigated. The sample was liquid, 1 cm thick and evenly distributed. As seen in Fig. 3C, the optical transparency of F127-OSA hydrogel at a concentration of 14 % reached 88.9 % at wavelengths above 600 nm. The gel's optical transparency somewhat decreased when its concentration was raised. However, F127-OSA hydrogels displayed an optical transparency of 72 % at wavelengths above 600 nm, even at concentrations as high as 20 %. In addition, B16-F10 mouse melanoma hypermetastasis cells were used to detect in vitro toxicity of F127-OSA thermosensitive gel. High concentrations of DMSO were cytotoxic and limited cell survival, so a cell medium containing 5 % DMSO was utilized as a positive control [30]. As shown in Fig. 3D, cells in the normal control group and the F127-OSA

thermosensitive gel group survived normally, with no significant difference in cell viability, while those in the positive group significantly decreased. These results indicate that F127-OSA thermosensitive gel has high light transmittance, negligible cytotoxicity and has good biological application potential.

3.6. Efficacy of BMP4 thermosensitive gel on CNV

CNV can be induced by a number of injuries such as trauma, infection, and chemical burns. Suture models are more stable than alkali burn models in that they can better preserve ocular tissue and do not result in perforations that might affect CNV measurement [31]. Therefore, in this study, we induced CNV formation in rats via sutures. In order to dynamically monitor the change of CNV after modeling and the inhibition impact of BMP4 dissolved in conventional solvent and F127-OSA thermosensitive hydrogel on CNV were compared. On the 3rd, 5th and 7th day after modeling, slit lamp was utilized to evaluate the CNV status (Fig. 4A). The length and area of CNV gradually grew with the extension of the stimulation time. On Day 5, the corneal rate-limiting barrier and tear secretion may interfere with BMP4 eye drops, preventing them from completely inhibiting CNV [32,33]. Poloxamer, however, exhibited histocompatibility, slow release, and good adherence. Loading BMP4 in F127-OSA thermosensitive hydrogel could prolong the residence time of

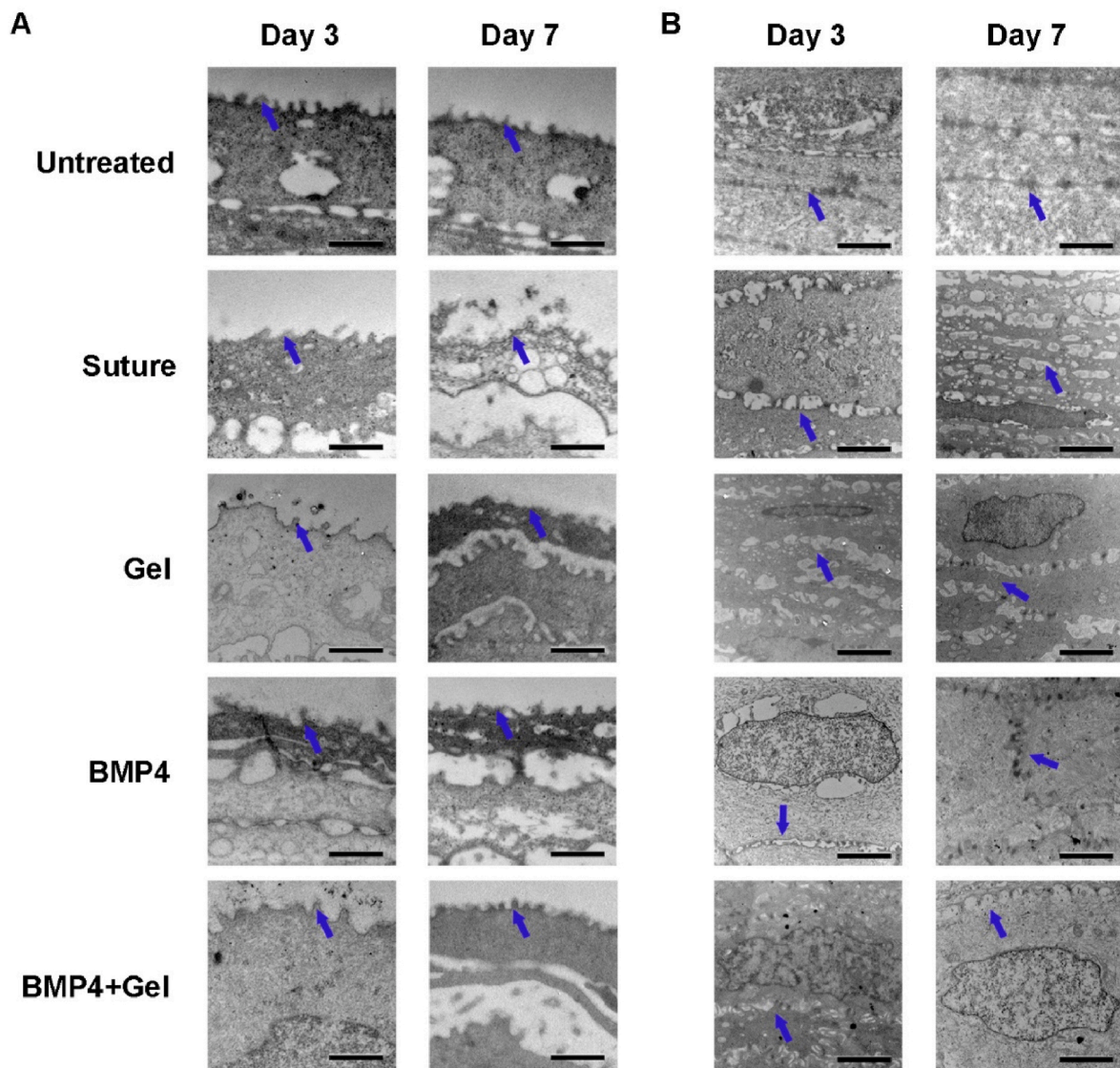


Fig. 6. The morphology of untreated group, suture group, gel group, BMP4 group, BMP4+gel group under TEM at Day 3 and 7 (n = 5). (A) the morphology of epithelial microvillus; (B) the morphology of epithelial superficial cells and intercellular junctions. Scale bars = 1 μm ($\times 8000$).

BMP4 on the ocular surface and promote the passage of hydrophilic BMP4 through the corneal lipid barrier [34], thus better inhibiting the formation of CNV (Fig. 4B and C). The microscopic structure of cornea was also changed after corneal suture and BMP4 dropping. We believe that the changes in protein and microstructure at day 3 of eye BMP4 and BMP4 in F127-OSA thermosensitive hydrogel were not enough to cause changes in CNV length and area. When eye BMP4 and BMP4 in F127-OSA thermosensitive hydrogel were dropped at day 5, the accumulated quantitative changes caused qualitative changes in CNV length and area, so there was a statistical difference at day 5. However, the stimulation of the sutures on the cornea always existed, CNV growth was more and more vigorous, and the inhibitory effect of BMP4 on CNV was gradually weakened, so the effect was not significant at 7 days, and then the dose and frequency of BMP4 dropping were considered to be increased before detection. This also provides more possibilities for the application of BMP4 thermosensitive hydrogel.

3.7. BMP4 thermosensitive hydrogel inhibits corneal edema and aberrant proliferation of corneal epithelial cells

The thickness of the corneal epithelium and the configuration of the epithelial cells might serve as indicators of corneal inflammation. The

corneal epithelium is accompanied by aberrant thickening in infectious keratitis [35,36], epithelial basement membrane dystrophy [37], mutations in destrin [38], and other disorders. In this study, we showed the effect of BMP4 thermosensitive hydrogel on corneal epithelial cell thickness and epithelial cell configuration by HE staining. The corneal epithelial cells in the untreated group were well stratified and organized, as seen in Fig. 5A. The columnar-arranged basal cells progressively differentiated into wing cells and superficial cells as they rose to the surface. Both the suture group and the gel group's corneal epithelial cells exhibited aberrant growth and disorganized organization. The aberrant proliferation and irregular arrangement of corneal epithelial cells could be inhibited by BMP4 eyedrops and BMP4 thermosensitive hydrogel. Additionally, the corneal epithelium's thickness dramatically increased after suture and continued to grow with longer stimulation periods. At all time periods, BMP4 eye drops and BMP4 thermosensitive hydrogel dramatically decreased corneal epithelial thickness, reduced corneal edema, and returned corneal thickness to normal levels. BMP4 thermosensitive hydrogel performed better on Day 5 than BMP4 eye drops did (Fig. 5B–D).

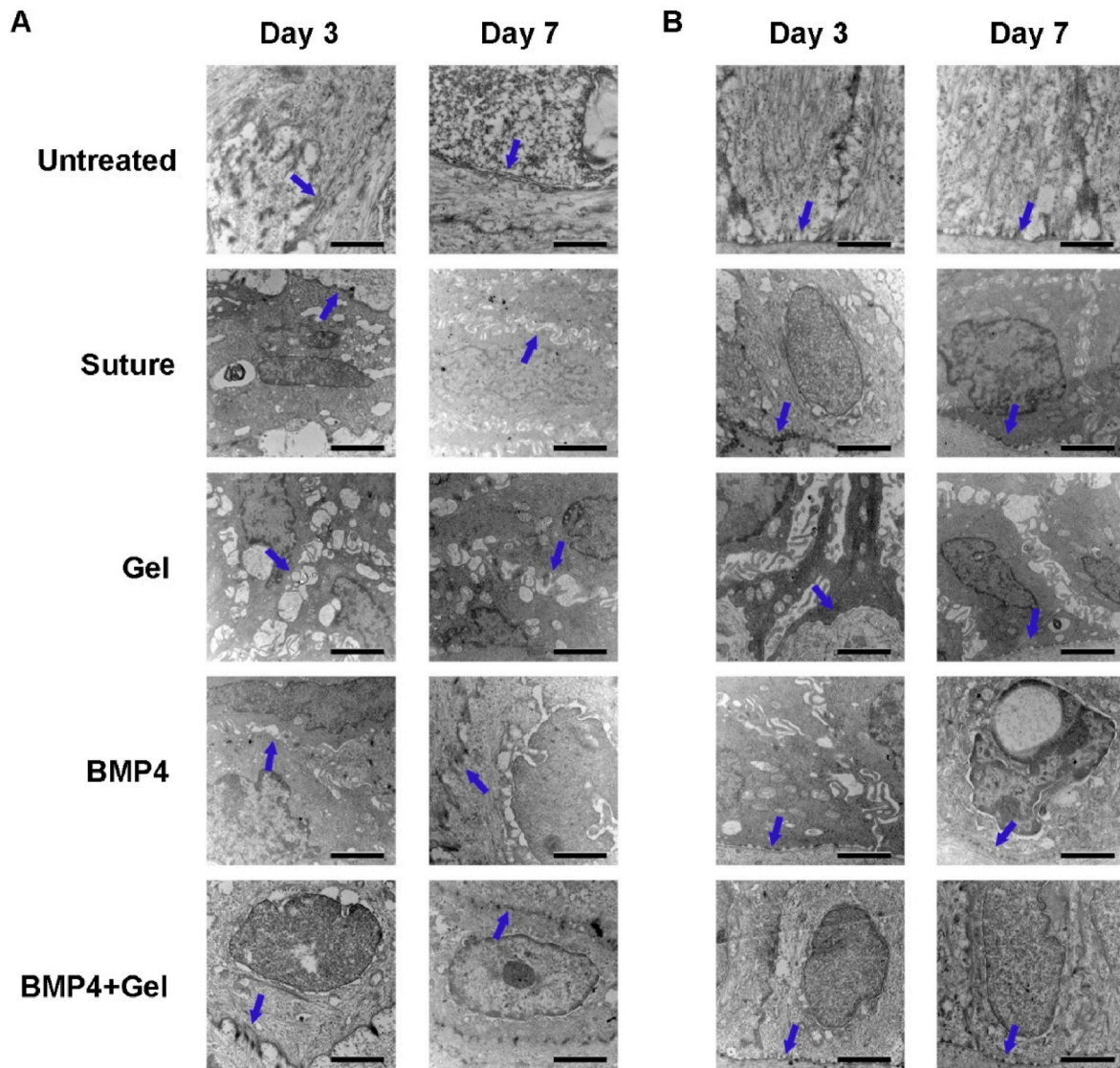


Fig. 7. The morphology of untreated group, suture group, gel group, BMP4 group, BMP4+gel group under TEM at Day 3 and 7 ($n = 5$). (A) the morphology of epithelial wing cells and intercellular junctions; (B) the morphology of epithelial basal cells, basement membrane, and hemidesmosomes. Scale bars = $1 \mu\text{m}$ ($\times 8000$).

3.8. BMP4 thermosensitive hydrogel restores the corneal epithelium's ultrastructural alterations brought on by CNV

The corneal epithelial barrier, mostly composed of AJCs and epithelial basement membrane, serves as the first line of protection for the ocular surface [39–41]. In order to investigate the healing effect of BMP4 on the corneal epithelial barrier from a microscopic perspective, the corneal epithelium of each group was observed by TEM on the 3rd and 7th day following the modeling. The corneal epithelial microvilli were numerous and organized in the untreated group, but they were flat, with apparent shedding and fusion, in the suture group and the gel control group. BMP4 eye drops and BMP4 thermosensitive hydrogel could improve the morphology and arrangement of epithelial cells and repair damaged microvilli (Fig. 6A).

Studies have shown that the injury of corneal epithelium AJCs can aggravate the progression of corneal disease while its restoration may aid to rearrange the corneal epithelium and delay the progression of corneal diseases [9]. Thus, we investigated the BMP4 thermosensitive gel's ability to repair different epithelial cells and intercellular junctions. Fig. 6B and 7A revealed that the superficial cells and wing cells in the untreated group possessed tight intercellular junctions, complete nuclei

and nuclear membranes, dense chromatin, and typical cell structures. The intercellular space was noticeably larger in the suture group, the intercellular junctions were disrupted, the chromatin was aberrant, the nuclear membrane was broadened, and the cytoplasm was focally lysed, along with an expansion of the rough endoplasmic reticulum and mitochondrial swelling. However, BMP4 eye drops and BMP4 thermosensitive hydrogel could be used to heal the aforementioned damage, with the thermosensitive hydrogel having a greater repair outcome than the eye drops.

The hemidesmosomes that exist between the corneal epithelium's basal cells and the basement membrane are also crucial for maintaining the corneal epithelium's structural integrity [42,43]. In the control group, the basal cells were evenly spaced, the hemidesmosomes were firmly connected, and the basement membrane was continuous. Following suture, the basement membrane was ruptured and the number of hemidesmosomes was greatly decreased. BMP4 thermosensitive hydrogel and BMP4 eye drops might be used to restore the integrity of the basement membrane and the stability of the hemidesmosomes (Fig. 7B). Studies have revealed that the basement membrane's filtration function and the regulatory effect of basement membrane proteins on the integrity of intercellular junctions help to resist pathogen invasion

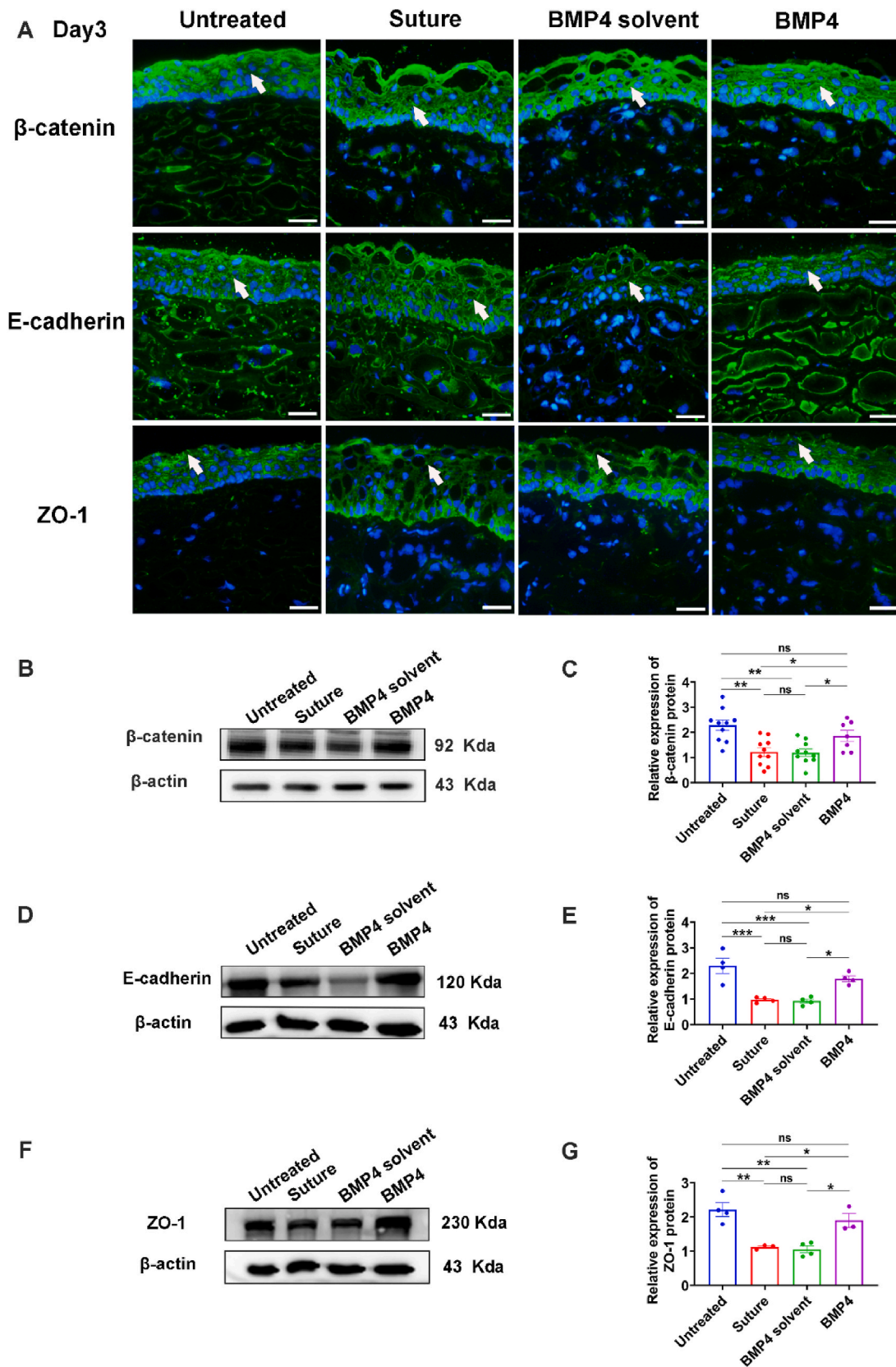


Fig. 8. Therapeutic effect of BMP4 eye drops on AJs. (A) immunofluorescence staining of corneal epithelial tight junction protein ZO-1 and adherens junction proteins β -catenin and E-cadherin in untreated group, suture group, BMP4 solvent group and BMP4 group at Day 3. Scale bars = 20 μ m (\times 400); (B) representative western blot analysis of β -catenin in corneal epithelium at Day 3. (C) the expression of β -catenin in corneal epithelium at Day 3. (D) representative western blot analysis of E-cadherin in corneal epithelium at Day 3. (E) the expression of E-cadherin in corneal epithelium at Day 3. (F) representative western blot analysis of ZO-1 expression in corneal epithelium at Day 3. (G) the expression of ZO-1 in corneal epithelium at Day 3. n = 6, results were presented as means \pm SEM. *P < 0.05, **P < 0.01, and ***P < 0.001.

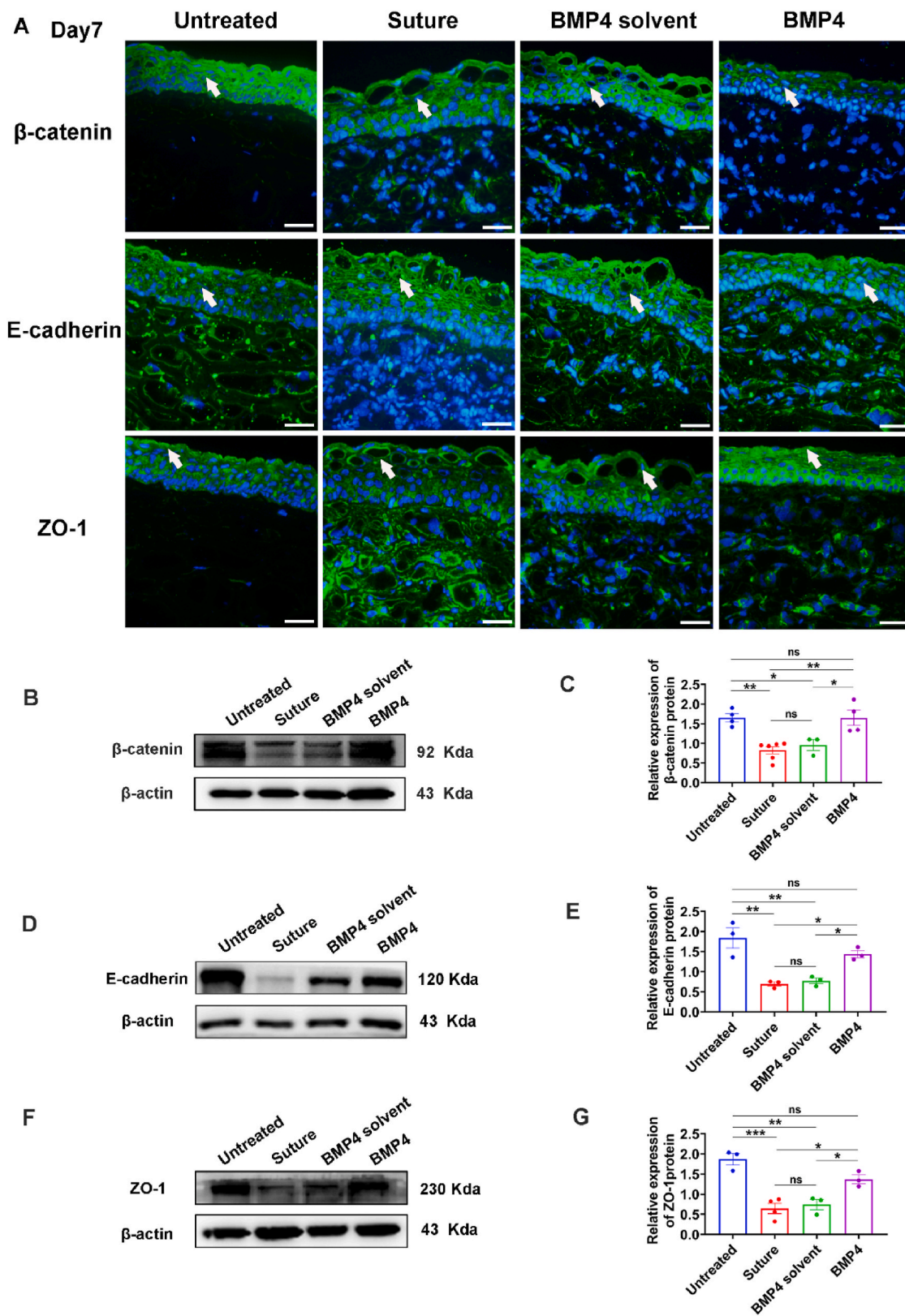


Fig. 9. Therapeutic effect of BMP4 eye drops on AJCs. (A) immunofluorescence staining of corneal epithelial tight junction protein ZO-1 and adherens junction proteins β-catenin and E-cadherin in untreated group, suture group, BMP4 solvent group and BMP4 group at Day 7. Scale bars = 20 μm (× 400); (B) representative western blot analysis of β-catenin in corneal epithelium at Day 7. (C) the expression of β-catenin in corneal epithelium at Day 7. (D) representative western blot analysis of E-cadherin in corneal epithelium at Day 7. (E) the expression of E-cadherin in corneal epithelium at Day 7. (F) representative western blot analysis of ZO-1 expression in corneal epithelium at Day 7. (G) the expression of ZO-1 in corneal epithelium at Day 7. n = 6, results were presented as means ± SEM. *P < 0.05, **P < 0.01, and ***P < 0.001.

into the corneal stroma [44]. In order to assist basal cells in migrating to the lesion and repairing the corneal epithelium's structure and function after injury, the basement membrane undergoes remodeling. Therefore, the healing of corneal epithelial damage benefits from the restoration of corneal epithelial basement membrane and hemidesmosomes. In this study, we showed that both BMP4 eye drops and BMP4 thermosensitive hydrogel could repair the damage of corneal epithelial microvilli, epithelial cells, AJCs, and basement membranes, and the healing effect of BMP4 thermosensitive hydrogel was better.

3.9. BMP4 can repair corneal epithelial AJCs

It is yet unknown how corneal epithelial AJC damage and healing relate to the development of CNV. Tight and adherens connexin abnormalities are frequently present alongside CNV development, and their malfunction promotes CNV development [45]. By using immunofluorescence and western blot analysis, we explored alterations in the tight junction protein ZO-1 and adherens junction proteins E-cadherin and β -catenin after 3 and 7 days of modeling in order to better understand the mechanism by which BMP4 inhibits CNV. Tight junctions are complexes composed of a variety of transmembrane proteins such as occludin and claudin, membrane related proteins such as ZO-1 and ZO-2, and actin, among which ZO-1 is often used as a sign of tight junctions [46,47]. Adherens junctions are mainly composed of the transmembrane glycoproteins' cadherin family and catenin family, which can promote the formation of tight junctions and stabilize barrier function [48,49]. Therefore, we reflected the changes of AJCs by the changes of ZO-1, E-cadherin and β -catenin.

Fig. 8A–G showed that the connections between corneal epithelial cells in the suture group and the solvent control group were loose and vacuolated after 3 days of modeling, and the quantity of intercellular junctions was dramatically decreased. The cells were organized neatly, and the intercellular junctions were tight after BMP4 eye drops were applied. The expression levels of ZO-1, E-cadherin, and β -catenin were also considerably lower in the suture group and the solvent control group than those in the control group, while BMP4 eye drops could dramatically raise the expression levels of the aforementioned proteins. The same impacts and patterns persisted after 7 days of modeling (Fig. 9A–G). These findings indicated that suture induced CNV formation caused damage to AJCs, which could be repaired by BMP4, suggesting that BMP4 thermosensitive hydrogel may inhibit CNV formation by repairing AJCs.

4. Conclusions

In this study, we report the development of F127-OSA thermosensitive hydrogel loaded with BMP4 and investigated the inhibitory effect of this hydrogel on CNV and its mechanism in vivo. The hydrogel provides more possibilities for the use of BMP4 thermosensitive hydrogel since it had excellent slow-release and biocompatibility, high light transmittance, and could significantly reduce the dosage of poloxamer and production costs when compared to traditional gel. This study proved that BMP4 thermosensitive hydrogel had a superior inhibitory impact on CNV compared to BMP4 eye drops. Additionally, the hydrogel might reduce inflammatory response and aid in corneal epithelial healing. AJCs were damaged during the development of CNV, and BMP4 thermosensitive hydrogel was able to prevent the development of CNV by mending the harmed AJCs. In conclusion, this study identifies the mechanism by which BMP4 thermosensitive hydrogel inhibits CNV and proves that F127-OSA hydrogel loaded with BMP4 is a potential new drug for the treatment of CNV.

Fundings

This work was supported by the Jilin Province Health Science and Technology Ability Promotion Project [grant number 2021JC015]; the

Jilin University Interdisciplinary Training Program for Young Teachers and Students [grant number 2022-JCCK-28]; the Jilin Province Natural Science Foundation [grant number YDZJ202301ZYTS067]; and the Mechanism of Inhibition of Corneal Neovascularization by BMP4 [grant number 3R2196623429]; Shanghai General Hospital [grant number 02.06.01.23.171].

Ethics approval and consent to participate

The animal study protocol was approved by the Ethics Committee of Jilin University.

CRediT authorship contribution statement

Weijin Nan: Conceptualization, Formal analysis, Methodology. **Sitong Shen:** Data curation, Methodology, Writing - original draft. **Yongyan Yang:** Data curation, Methodology, Writing - original draft. **Meiliang Wu:** Data curation. **Yuxi He:** Funding acquisition, Supervision. **Ruiting Zhang:** Software. **Xuejun Cui:** Supervision, Writing - review & editing. **Yan Zhang:** Funding acquisition, Supervision, Writing - review & editing.

Declaration of competing interest

No conflict of interest exists in the submission of this manuscript, and manuscript is approved by all authors for publication. I would like to declare on behalf of my co-authors that the work described was original research that has not been published previously, and not under consideration for publication elsewhere, in whole or in part.

Data availability

Data will be made available on request.

Acknowledgments

We thank Biorender (<https://biorender.com/>) and Yifan Bao from University of Vienna for helping provide the figures in this manuscript.

References

- [1] Q. Li, X. Hua, L. Li, X. Zhou, Y. Tian, Y. Deng, M. Zhang, X. Yuan, W. Chi, AIP1 suppresses neovascularization by inhibiting the NOX4-induced NLRP3/NLRP6 imbalance in a murine corneal alkali burn model, *Cell Commun. Signal. : CCS* 20 (1) (2022) 59.
- [2] M.P. Nicholas, N. Mysore, Corneal neovascularization, *Exp. Eye Res.* 202 (2021) 108363.
- [3] K. Yi, Y. Yang, Y. Yuan, Y. Xiang, S. Zhou, Impaired autophagy causes severe corneal neovascularization, *Cells* 11 (23) (2022) 3895.
- [4] K.K. Yeung, H.J. Yang, A.L. Nguyen, B.A. Weissman, Critical contact lens oxygen transmissibility and tear lens oxygen tension to preclude corneal neovascularization, *Eye Contact Lens* 44 (Suppl 1) (2018) S291–s295.
- [5] J.H. Wang, C.L. Tseng, F.L. Lin, J. Chen, E.H. Hsieh, S. Lama, Y.F. Chuang, S. Kumar, L. Zhu, M.B. McGuinness, et al., Topical application of TAK1 inhibitor encapsulated by gelatin particle alleviates corneal neovascularization, *Theranostics* 12 (2) (2022) 657–674.
- [6] Y. Han, L. Jiang, H. Shi, C. Xu, M. Liu, Q. Li, L. Zheng, H. Chi, M. Wang, Z. Liu, et al., Effectiveness of an ocular adhesive polyhedral oligomeric silsesquioxane hybrid thermo-responsive FK506 hydrogel in a murine model of dry eye, *Bioact. Mater.* 9 (2022) 77–91.
- [7] D. Roshandel, M. Eslani, A. Baradaran-Rafii, A.Y. Cheung, K. Kurji, S. Jabbehdari, A. Maiz, S. Jalali, A.R. Djalilian, E.J. Holland, Current and emerging therapies for corneal neovascularization, *Ocul. Surf.* 16 (4) (2018) 398–414.
- [8] M. Dong, G. Di, X. Zhang, Q. Zhou, W. Shi, Subconjunctival bevacizumab injection impairs corneal innervations and epithelial wound healing in mice, *Invest. Ophthalmol. Vis. Sci.* 58 (3) (2017) 1469–1477.
- [9] J. Hu, N. Gao, Y. Zhang, X. Chen, J. Li, F. Bian, W. Chi, Z. Liu, C.S. de Paiva, S. C. Pflugfelder, et al., IL-33/ST2/IL-9/IL-9R signaling disrupts ocular surface barrier in allergic inflammation, *Mucosal Immunol.* 13 (6) (2020) 919–930.
- [10] Y. Yang, B. Gong, Z.Z. Wu, P. Shuai, D.F. Li, L.L. Liu, M. Yu, Inhibition of microRNA-129-5p expression ameliorates ultraviolet ray-induced corneal epithelial cell injury via upregulation of EGFR, *J. Cell. Physiol.* 234 (7) (2019) 11692–11707.

- [11] P. Lu, G. Liu, Inhibition of experimental corneal neovascularization by the tight junction protein Zonula Occludens 1, *Eur. J. Immunol.* 49 (2019) 121, 121.
- [12] G.B. Park, D. Kim, Y.S. Kim, S. Kim, H.K. Lee, J.W. Yang, D.Y. Hur, The Epstein-Barr virus causes epithelial-mesenchymal transition in human corneal epithelial cells via Syk/src and Akt/Erk signaling pathways, *Invest. Ophthalmol. Vis. Sci.* 55 (3) (2014) 1770–1779.
- [13] Y. Zhang, M.K. Call, L.K. Yeh, H. Liu, T. Kochel, L.J. Wang, P.H. Chu, M.M. Taketo, J.V. Jester, W.W. Kao, et al., Aberrant expression of a beta-catenin gain-of-function mutant induces hyperplastic transformation in the mouse cornea, *J. Cell Sci.* 123 (Pt 8) (2010) 1285–1294.
- [14] R.K. Baboota, M. Blüher, U. Smith, Emerging role of bone morphogenetic protein 4 in metabolic disorders, *Diabetes* 70 (2) (2021) 303–312.
- [15] R. Guan, L. Yuan, J. Li, J. Wang, Z. Li, Z. Cai, H. Guo, Y. Fang, R. Lin, W. Liu, et al., Bone morphogenetic protein 4 inhibits pulmonary fibrosis by modulating cellular senescence and mitophagy in lung fibroblasts, *Eur. Respir. J.* 60 (6) (2022) 2102307.
- [16] S. Shen, S. Wang, Y. He, H. Hu, B. Yao, Y. Zhang, Regulation of bone morphogenetic protein 4 on epithelial tissue, *Journal of cell communication and signaling* 14 (3) (2020) 283–292.
- [17] H. Hu, S. Wang, Y. He, S. Shen, B. Yao, D. Xu, X. Liu, Y. Zhang, The role of bone morphogenetic protein 4 in corneal injury repair, *Exp. Eye Res.* 212 (2021) 108769.
- [18] C. Zhao, L. Zhou, M. Chiao, W. Yang, Antibacterial hydrogel coating: strategies in surface chemistry, *Adv. Colloid Interface Sci.* 285 (2020) 102280.
- [19] H. Cao, L. Duan, Y. Zhang, J. Cao, K. Zhang, Current hydrogel advances in physicochemical and biological response-driven biomedical application diversity, *Signal Transduct. Targeted Ther.* 6 (1) (2021) 426.
- [20] L. Xu, Y. Zhang, S. Wang, H. Hu, S. Zhong, S. He, Y. Dou, Z. Li, X. Cui, Thermoresponsive gel for sustained release of BMP4 to inhibit corneal neovascularization, *Colloids and surfaces B, Biointerfaces* 194 (2020) 111167.
- [21] Z. Wei, J.H. Yang, Z.Q. Liu, F. Xu, J.X. Zhou, M. Zrinyi, Y. Osada, Y.M. Chen, Novel biocompatible polysaccharide-based self-healing hydrogel, *Adv. Funct. Mater.* 25 (9) (2015) 1352–1359.
- [22] Z. Emami, M. Ehsani, M. Zandi, R. Foudazi, Controlling alginate oxidation conditions for making alginate-gelatin hydrogels, *Carbohydr. Polym.* 198 (2018) 509–517.
- [23] M.J. Moura, M.H. Gil, M.M. Figueiredo, Delivery of cisplatin from thermosensitive co-cross-linked chitosan hydrogels, *Eur. Polym. J.* 49 (9) (2013) 2504–2510.
- [24] W. Zhang, Y. Shi, Y. Chen, J. Ye, X. Sha, X. Fang, Multifunctional Pluronic P123/F127 mixed polymeric micelles loaded with paclitaxel for the treatment of multidrug resistant tumors, *Biomaterials* 32 (11) (2011) 2894–2906.
- [25] H. Zheng, S. Wang, F. Cheng, X. He, Z. Liu, W. Wang, L. Zhou, Q. Zhang, Bioactive anti-inflammatory, antibacterial, conductive multifunctional scaffold based on MXene@CeO₂ nanocomposites for infection-impaired skin multimodal therapy, *Chem. Eng. J.* (2021) 424.
- [26] Santhanam S, Liang J, Struckhoff J, Hamilton PD, Ravi N: Biomimetic hydrogel with tunable mechanical properties for vitreous substitutes. (1878-7568 (Electronic)):327-337.
- [27] K. Al Khateb, E.K. Ozhmukhametova, M.N. Mussin, S.K. Seilkhanov, T. K. Rakhypbekov, W.M. Lau, V.V. Khutoryanskiy, In situ gelling systems based on Pluronic F127/Pluronic F68 formulations for ocular drug delivery, *Int. J. Pharm.* 502 (1–2) (2016) 70–79.
- [28] S. Yu, X. Zhang, G. Tan, L. Tian, D. Liu, Y. Liu, X. Yang, W. Pan, A novel pH-induced thermosensitive hydrogel composed of carboxymethyl chitosan and poloxamer cross-linked by glutaraldehyde for ophthalmic drug delivery, *Carbohydr. Polym.* 155 (2017) 208–217.
- [29] X. Zhao, S. Li, X. Du, W. Li, Q. Wang, D. He, J. Yuan, Natural polymer-derived photocurable bioadhesive hydrogels for sutureless keratoplasty, *Bioact. Mater.* 8 (2022) 196–209.
- [30] K. Kim, S.E. Lee, Combined toxicity of dimethyl sulfoxide (DMSO) and vanadium towards zebrafish embryos (*Danio rerio*): unexpected synergistic effect by DMSO, *Chemosphere* 270 (2021) 129405.
- [31] P. Wang, P. Hao, X. Chen, L. Li, Y. Zhou, X. Zhang, L. Zhu, M. Ying, R. Han, L. Wang, et al., Targeting HMGB1-NFκB Axis and miR-21 by glycyrrhizin: role in amelioration of corneal injury in a mouse model of alkali burn, *Front. Pharmacol.* 13 (2022) 841267.
- [32] T. Zhou, K. Yan, Y. Zhang, L. Zhu, Y. Liao, X. Zheng, Y. Chen, X. Li, Z. Liu, Z. Zhang, Fenofibrate suppresses corneal neovascularization by regulating lipid metabolism through PPARα signaling pathway, *Front. Pharmacol.* 13 (2022) 1000254.
- [33] D. Bennet, Z. Estlack, T. Reid, J. Kim, A microengineered human corneal epithelium-on-a-chip for eye drops mass transport evaluation, *Lab Chip* 18 (11) (2018) 1539–1551.
- [34] S.K. Motwani, S. Chopra, S. Talegaonkar, K. Kohli, F.J. Ahmad, R.K. Khar, Chitosan-sodium alginate nanoparticles as submicroscopic reservoirs for ocular delivery: formulation, optimisation and in vitro characterisation, *Eur. J. Pharm. Biopharm. : official journal of Arbeitsgemeinschaft fur Pharmazeutische Verfahrenstechnik eV* 68 (3) (2008) 513–525.
- [35] Z. Fathalla, W.W. Mustafa, H. Abdelkader, H. Moharram, A.M. Sabry, R.G. Alany, Hybrid thermosensitive-mucoadhesive in situ forming gels for enhanced corneal wound healing effect of L-carnosine, *Drug Deliv.* 29 (1) (2022) 374–385.
- [36] L. Li, Y. Li, X. Li, Y. Xia, E. Wang, D. Gong, G. Chen, L. Yang, K. Zhang, Z. Zhao, et al., HSV-1 infection and pathogenesis in the tree shrew eye following corneal inoculation, *J. Neurovirol.* 26 (3) (2020) 391–403.
- [37] A. Levy, C. Georgeon, J. Knoeri, M. Tourabaly, L. Leveziel, N. Bouheraoua, V. M. Borderie, Corneal epithelial thickness mapping in the diagnosis of ocular surface disorders involving the corneal epithelium: a comparative study, *Cornea* 41 (11) (2022) 1353–1361.
- [38] T.P. O'Brien, Q.J. Li, F. Sauerburger, V.E. Reviglio, T. Rana, M.F. Ashraf, The role of matrix metalloproteinases in ulcerative keratolysis associated with perioperative diclofenac use, *Ophthalmology* 108 (4) (2001) 656–659.
- [39] S.V. Kawakami-Schulz, A.M. Verdoni, S.G. Sattler, A. Ikeda, S. Ikeda, Differences in corneal phenotypes between destrin mutants are due to allelic difference and modified by genetic background, *Mol. Vis.* 18 (2012) 606–616.
- [40] Z. Barry, B. Park, T.W. Corson, Pharmacological potential of small molecules for treating corneal neovascularization, *Molecules* 25 (15) (2020).
- [41] N. Yokoi, A. Komuro, K. Nishida, S. Kinoshita, Effectiveness of hyaluronan on corneal epithelial barrier function in dry eye, *Br. J. Ophthalmol.* 81 (7) (1997) 533–536.
- [42] M.D. Kottke, E. Delva, A.P. Kowalczyk, The desmosome: cell science lessons from human diseases, *J. Cell Sci.* 119 (Pt 5) (2006) 797–806.
- [43] I. Alarcon, C. Tam, J.J. Mun, J. LeDue, D.J. Evans, S.M. Fleiszig, Factors impacting corneal epithelial barrier function against *Pseudomonas aeruginosa* traversal, *Invest. Ophthalmol. Vis. Sci.* 52 (3) (2011) 1368–1377.
- [44] T.H. van Essen, L. van Zijl, T. Possemiers, A.A. Mulder, S.J. Zwart, C.H. Chou, C. C. Lin, H.J. Lai, G.P.M. Luyten, M.J. Tassignon, et al., Biocompatibility of a fish scale-derived artificial cornea: cytotoxicity, cellular adhesion and phenotype, and in vivo immunogenicity, *Biomaterials* 81 (2016) 36–45.
- [45] D.J. Evans, S.M. Fleiszig, Why does the healthy cornea resist *Pseudomonas aeruginosa* infection? *Am. J. Ophthalmol.* 155 (6) (2013) 961–970, e962.
- [46] S. Chatterjee, Y. Wang, M.K. Duncan, U.P. Naik, Junctional adhesion molecule-A regulates vascular endothelial growth factor receptor-2 signaling-dependent mouse corneal wound healing, *PLoS One* 8 (5) (2013) e63674.
- [47] E.E. Schneeberger, R.D. Lynch, The tight junction: a multifunctional complex, *Am. J. Physiol. Cell Physiol.* 286 (6) (2004) C1213–C1228.
- [48] B. Lee, K.M. Moon, C.Y. Kim, Tight junction in the intestinal epithelium: its association with diseases and regulation by phytochemicals, *J. Immunol. Research* 2018 (2018) 2645465.
- [49] R.M. Mège, N. Ishiyama, Integration of cadherin adhesion and cytoskeleton at adherens junctions, *Cold Spring Harbor Perspect. Biol.* 9 (5) (2017) a028738.

Abbreviations

CNV: corneal neovascularization
 BMP4: bone morphogenetic protein 4
 F127-OSA: poloxamer-oxidized sodium alginate
 AJCs: apical junctional complexes
 VEGF-A: vascular endothelium growth factor A
 SA: sodium alginate
 NaIO₄: sodium periodate
 CDI: N, N'-Carbonyldiimidazole
 FTIR: Fourier transform infrared spectroscopy
 PEO: polyethylene oxide
 PPO: propylene oxide
 BSA: bovine serum